Nanoscale

COMMUNICATION

View Article Online
View Journal | View Issue



Cite this: *Nanoscale*, 2019, **11**, 5868

Received 4th December 2018,
Accepted 5th March 2019

DOI: 10.1039/c8nr09780a

rsc.li/nanoscale



# Pressure-induced fluorescence enhancement of $FA_\alpha PbBr_{2+\alpha}$ composite perovskites†

Lan Anh Thi Nguyen, [a,b] Duong Nguyen Minh,[c] Ye Yuan,[d] Sudeshna Samanta,[b,d] Lin Wang,[d] Dongzhou Zhang,[e] Naohisa Hirao,[f] Jaeyong Kim *[a,b] and Youngjong Kang *[c,g]

**$FA_\alpha PbBr_{2+\alpha}$ composite perovskites consisting of 0D $FA_4PbBr_6$ and 3D $FAPbBr_3$ have been synthesized by a solid state reaction. Due to the endotaxy passivation of $FAPbBr_3$ by $FA_4PbBr_6$, $FAPbBr_3$ crystals were stably deformed without agglomeration from the cubic to the orthorhombic structure by compression, which led to a significant PL enhancement.**

Metal halide perovskites have received increasing attention due to their outstanding optical and electrical properties such as broad optical absorption, high photoluminescence quantum yield (PLQY) with broad color tunability, long charge diffusion length and high mobility.[1–7] The general formula of perovskites is $A_\alpha BX_{2+\alpha}$, where A, B, and X are monovalent cation, divalent metals such as $Pb^{2+}$, and halogen anions such as $Cl^-$, $Br^-$, and $I^-$, respectively. Inorganic $Cs^+$ ions or organic ammonium including methylammonium (MA, $CH_3NH_3^+$) or formamidinium (FA, $CH(NH_2)_2^+$) are often used for the cation $A^+$. In this case, $\alpha$ can be varied from 1 to 4. For the case of $\alpha$ = 1 ($ABX_3$), it forms a typical three-dimensional (3D) structure, where the $A^+$ is surrounded by the network of corner sharing $[BX_6]^{4-}$ octahedra. Increasing $\alpha$ leads to the formation of the lower dimensional structures where the octahedral network is separated by the cation $A^+$, and ultimately zero-dimensional (0D) perovskites ($A_4BX_6$) are formed when $\alpha$ is increased to $\alpha$ = 4. The 0D perovskite structure consists of the isolated octahedra interspersed with the cations.[8,9] Among them, 3D perovskite nanoparticles have been extensively investigated as a promising material for light emitters. They offer wide bandgap tunability simply by changing their elemental composition. However, their very low PLQY in the solid state (typically less than 1%) as compared to their high PLQY in solution (~90%) hampers their application in LEDs.[10,11] While 0D perovskites have not been investigated as extensively as 3D perovskites, they are also of interest due to their strong quantum confinement and high stability. Since metal–halide-comprised octahedra are spatially confined, 0D perovskites show high exciton binding energy which is efficient for exhibiting high PLQY. Unlike typical 3D perovskites, 0D perovskite nanocrystals exhibit comparable PLQY in both solution (65%) and in the solid state (56%).[9,12,13]

While the optical and electrical properties of perovskites have been tuned by changing the halide $X^-$ or the size of nanoparticles,[11,14] they can also be altered by applying high pressure.[15] For example, the recent studies show that applying high pressure on 3D perovskites led to piezochromism, conductivity enhancement and/or phase transitions because of the bond length contraction and octahedral distortion in crystal structures.[15–19] However, the photoluminescence properties of perovskites were significantly deteriorated under high pressure conditions because of losing their quantum confinement by agglomeration.[19,20]

Herein, we report dramatic photoluminescence enhancement in a mixture of 0D and 3D formamidinium lead bromide perovskite ($FA_4PbBr_6$/$FAPbBr_3$) (hereafter named $FA_\alpha PbBr_{2+\alpha}$ composite perovskite) under high pressure in the order of giga-pascal (GPa). The decay of perovskite photoluminescence in the solid state or under pressure is known to be mainly due to the agglomeration of crystals. Hence some passivation techniques including polymer encapsulation and core–shell structures have been employed.[21,22] Recently, endotaxy passivation wherein crystals are covered with the same chemical elements but in different crystal structures was found to be very effective for stabilizing nanocrystals.[23,24] For example, Quan *et al.*

[a]*Department of Physics, Hanyang University, Seoul, 04763, Korea*
[b]*HYU-HPSTAR-CIS High Pressure Research Center, Hanyang University, Seoul, 04763, Korea. E-mail: kimjy@hanyang.ac.kr*
[c]*Department of Chemistry, Hanyang University, Seoul, 04763, Korea*
[d]*Center for High Pressure Science & Technology Advanced Research, Shanghai 201203, China*
[e]*Partnership for Extreme Crystallography, University of Hawaii at Manoa, Honolulu, HI 96822, USA*
[f]*Japan Synchrotron Radiation Research Institute, Hyogo 679-5198, Japan*
[g]*Research Institute for Natural Sciences and Institute of Nano Science and Technology, Hanyang University, Seoul04763, Korea. E-mail: youngjkang@hanyang.ac.kr*

†Electronic supplementary information (ESI) available. See DOI: 10.1039/c8nr09780a

found that the 3D $CsPbBr_3$ nanocrystals embedded in the 0D $Cs_4PbBr_6$ matrix exhibited a remarkably high PLQY in the solid state by endotaxy passivation.[25] Similarly, 3D $FAPbBr_3$ can be stably passivated with 0D $FA_4PbBr_6$ and *vice versa*, when their lattices match each other. In this case, both 0D and 3D crystals can be stably deformed under high pressure conditions without agglomeration, which leads to the enhancement of PLQY due to the increased binding energy by structural distortion. To this end, $FA_\alpha PbBr_{2+\alpha}$ composite perovskites were prepared and characterized under the high pressure conditions. Our experiments show that the PL intensity of $FA_\alpha PbBr_{2+\alpha}$ composite perovskites was enhanced by 21 times under the high pressure conditions compared with that under ambient conditions, and it remained stable over multiple compression cycles.

$FA_\alpha PbBr_{2+\alpha}$ composite perovskites were prepared by employing a solid state reaction. Briefly, the $PbBr_2$–DMSO complex was first prepared by following the procedures reported previously.[26] The completely dried $PbBr_2$–DMSO complex powder was then mixed with FABr powder in a glovebox. Upon mixing, the white powder instantaneously turned pale orange, and exhibited green fluorescence under UV (Fig. 1a, S1†). In contrast, the mixture of $PbBr_2$ and FABr barely showed PL under the same conditions (Fig. S1†). The results of synchrotron-based powder X-ray diffraction (XRD) data confirmed that the sample contained two different crystal structures, $FA_4PbBr_6$ ($R\bar{3}c$, $a = b = 13.07$ Å, $c = 18.45$ Å) and $FAPbBr_3$ perovskites ($Pm\bar{3}m$, $a = b = c = 5.99$ Å) (Fig. 1b). The refinement results of the general structure refinement system (GSAS) to the measured XRD data are presented in Fig. S2.† Based on the matching with the main diffracted peak positions and normalized amount of peak intensity, it was expected that $FA_4PbBr_6$ perovskite was dominant over the $FAPbBr_3$ one. Due to the relatively large excess amount of $FA_4PbBr_6$, $FAPbBr_3$ was expected to be embedded within the $FA_4PbBr_6$ matrix. In this case, endotaxy passivation of $FAPbBr_3$ by $FA_4PbBr_6$ was expected because of their close lattice matching (Table S3, Fig. S3†). Since the resulting $FA_\alpha PbBr_{2+\alpha}$ composite perovskites were easily hydrolyzed under ambient conditions, all experiments were performed under inert conditions. The PL spectrum of $FA_\alpha PbBr_{2+\alpha}$ composite perovskite was almost the same as that of pure $FAPbBr_3$ perovskite nanoparticles deposited on a Si substrate.[26,27] UV-Vis data also supported the formation of $FA_\alpha PbBr_{2+\alpha}$ composite perovskite. The absorbance spectra of the mixture showed the existence of a strong and narrow absorbance peak at 325 nm which originated from $FA_4PbBr_6$ perovskite (Fig. 3a),[28] and a gentle slope at 540 nm corresponding to the absorption peak of $FAPbBr_3$ (Fig. 1c and 3b).[26] All these data support well the formation of $FA_\alpha PbBr_{2+\alpha}$ composite perovskite by the simple solid-state reaction of $PbBr_2$–DMSO and FABr powders.

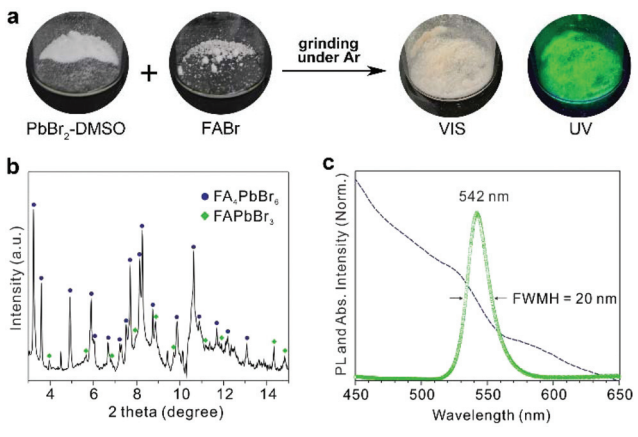


**Fig. 1** (a) Preparation of the $FA_\alpha PbBr_{2+\alpha}$ composite perovskite by a solid state mixing of $PbBr_2$–DMSO and FABr powders. Upon mixing, the mixtures exhibited strong green fluorescence under UV illumination. (b) XRD pattern of the $FA_\alpha PbBr_{2+\alpha}$ composite perovskite which shows that the resulting compound was a mixture of 0D $FA_4PbBr_6$ and 3D $FAPbBr_3$. The expected peak positions for 0D and 3D structures from the GSAS calculation are marked on the pattern. (c) PL and UV-Vis absorbance spectra of the $FA_\alpha PbBr_{2+\alpha}$ composite perovskite.

The high pressure experiments were carried out by using a symmetric diamond anvil cell (DAC). $FA_\alpha PbBr_{2+\alpha}$ composite perovskites were pressurized by silicon oil as a pressure medium in a DAC. Ruby was used as a pressure marker. PL and fluorescent optical microscope images of $FA_\alpha PbBr_{2+\alpha}$ composite perovskite were taken *in situ* while changing pressure (Fig. 2). Under ambient conditions, $FA_\alpha PbBr_{2+\alpha}$ composite perovskite showed a green fluorescence emission at $\lambda_{peak}$ = 542 nm. The PL spectrum corresponded to that of pure $FAPbBr_3$,[26] which suggests that PL of $FA_\alpha PbBr_{2+\alpha}$ composite perovskite was mainly due to $FAPbBr_3$. The green emission gradually turned orange with increasing the pressure until 2.0 GPa, and then turned back to green as the pressure increased further (Fig. 2). When the pressure increased further above 4.1 GPa, the fluorescence almost disappeared. After releasing the pressure, however, the sample recovered the green fluorescence. Such changes of photoemission color were almost the same as other previous reports on the pressure-induced PL changes of pure $FAPbBr_3$ perovskite.[16] In the aspect of PL intensity, however, the $FA_\alpha PbBr_{2+\alpha}$ composite perovskite represented different responses from other pure 3D perovskites under high-pressure.[19,20] While PL of pure 3D perovskites mostly decreased with the pressure, PL of the $FA_\alpha PbBr_{2+\alpha}$ composite perovskite gradually increased showing the maximum intensity at 2.0 GPa (Fig. 2). The PL enhancement factor ($f$) was $f = 21$ at 2.0 GPa, where $f$ was defined as the ratio of the PL intensity at a certain pressure to the intensity at 1 atm. Such dramatic enhancement of PL suggests that the agglomeration of the $FAPbBr_3$ perovskite was effectively restricted during the compression. With increasing the pressure, the PL peak consistently shifted to a longer wavelength ($\lambda_{peak}$ = 542–589 nm) until the pressure reached 2.0 GPa, followed by a blue-shift with the decrease of the intensity at the higher pressure (>2.0 GPa). The PL spectra persistently maintained the narrow bandwidth, full width at half maximum (FWHM) = 20 nm during the PL shift. The detailed information of the bandwidth and peak position of PL spectra with varying pressure is presented in Table S1.† Above 3.5 GPa,

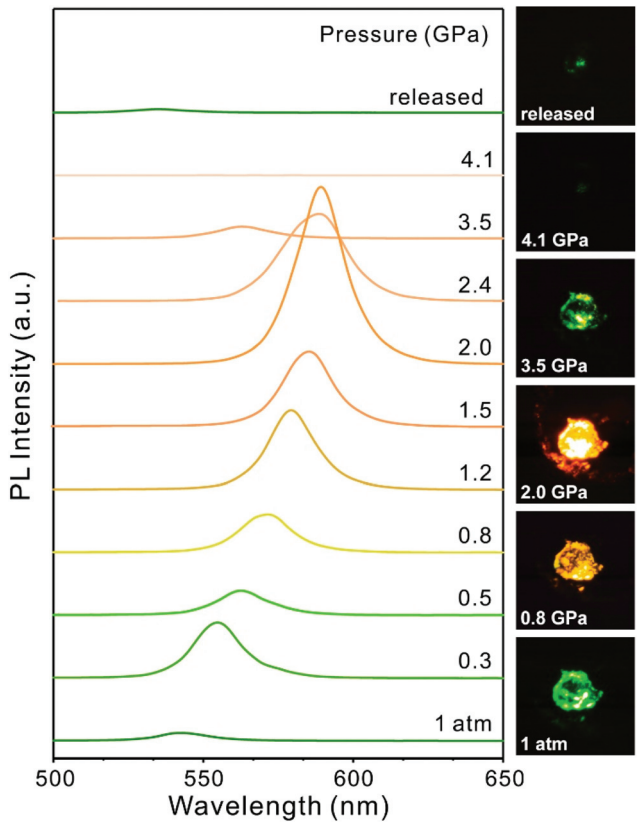


Fig. 2 Pressure-induced PL changes of the $FA_{\alpha}PbBr_{2+\alpha}$ composite perovskite. Spectra and fluorescent optical image of a $FA_{\alpha}PbBr_{2+\alpha}$ composite perovskite were taken *in situ* while increasing the pressure from 1 atm to 4.1 GPa.

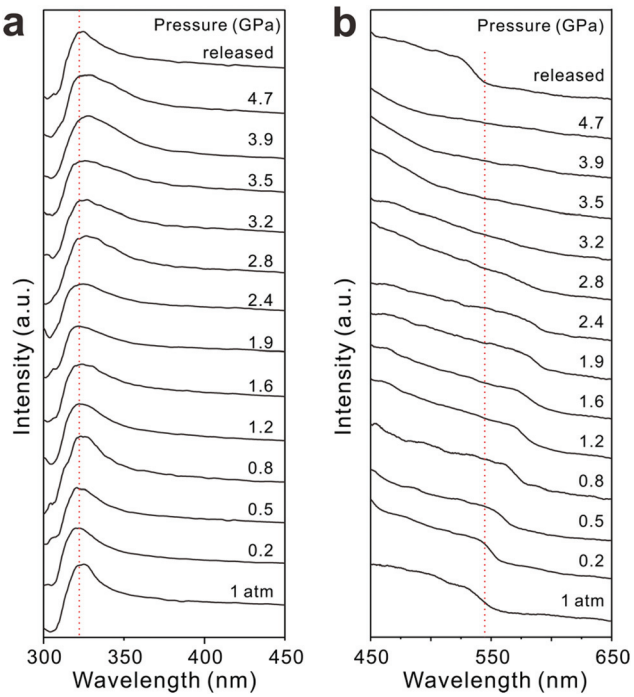


Fig. 3 UV-Vis absorbance spectra of the $FA_{\alpha}PbBr_{2+\alpha}$ composite perovskite as a function of the applied pressure. (a) The peak at 325 nm that originated from $FA_4PbBr_6$ was insensitive to the change of the pressure. (b) The band at 540 nm that originated from $FAPbBr_3$ was persistently shifted to the longer wavelength as the pressure increased to 2.4 GPa, and then the feature disappeared above 2.8 GPa. After releasing the pressure, the band was recovered, but shifted slightly to the shorter wavelength (535 nm).

PL almost disappeared presumably due to the pressure-induced amorphorization of $FAPbBr_3$.[16] It is noteworthy to mention that the pressure-induced PL enhancement was repeatable. After the first cycle of the compression, the $FA_{\alpha}PbBr_{2+\alpha}$ composite perovskite showed the same PL response during the subsequent second cycle. This result suggests that $FAPbBr_3$ perovskites were stably passivated without agglomeration by compression.

The pressure-induced phase transition of the $FA_{\alpha}PbBr_{2+\alpha}$ composite perovskite was also apparent in UV-Vis spectra. As shown in Fig. 3a, the absorbance peak at 325 nm corresponding to $FA_4PbBr_6$ was almost insensitive to the change of pressure up to 4.7 GPa. However, the $FAPbBr_3$ peak at 540 nm gradually shifted to a longer wavelength until 2.4 GPa ($\lambda_{peak}$ = 588 nm), and subsequently disappeared at higher pressure (>3.2 GPa) (Fig. 3b). After releasing the pressure, the band of $FAPbBr_3$ was recovered, but was slightly shifted to the shorter wavelength (535 nm). The values of optical bandgaps were estimated from UV-Vis spectra (Fig. S4†).[29] Due to the redshift of the absorbance edge during the compression, the bandgap was decreased.[16] The increase of the band gap after releasing the pressure indicates the formation of small or thin layered $FAPbBr_3$.[30–32]

To correlate the optical properties with the structure, *in situ* high pressure XRD patterns of $FA_{\alpha}PbBr_{2+\alpha}$ composite perovskite were analyzed as a function of pressure (Fig. 4). With increasing pressure, the main diffraction peaks of both $FAPbBr_3$ and $FA_4PbBr_6$ shifted to a higher angle. Results of GSAS refinement revealed that the crystal structure of $FA_4PbBr_6$ ($R\bar{3}c$, $a = b = 13.07$ Å, $c = 18.45$ Å) was retained but slightly distorted at 5.3 GPa. In contrast, the crystal structure of $FAPbBr_3$ exhibited strong pressure-dependent transitions: $Pm\bar{3}m$ ($a = b = c = 5.99$ Å) at 1 atm, $Im\bar{3}$ ($a = b = c = 11.12$ Å) at 0.8 GPa, and *Pnma* ($a = 8.18$ Å, $b = 11.44$ Å, $c = 8.49$ Å) at 2.0 GPa. These analyses indicate that the PL change by compression was mainly because of the pressure-induced transition of cubic to orthorhombic $FAPbBr_3$, which was induced by shrinking and tilting of $[PbBr_6]^{4-}$ octahedra.[16] In this case, $FA_4PbBr_6$ did not directly contribute to the PL enhancement, but was stabilized $FAPbBr_3$ by endotaxy passivation. After 3.0 GPa, the shape of the broad and weak peaks suggests the gradual amorphorization process, which was responsible for the disappearance of PL. The original $Pm\bar{3}m$ crystal structure of $FAPbBr_3$ was recovered after releasing the pressure to 1 atm (details shown in Fig. S2†). It was shown that the lattice mismatch was maintained low during the compression (Table S3†). After the pressure release, two crystals ($FAPbBr_3$

 

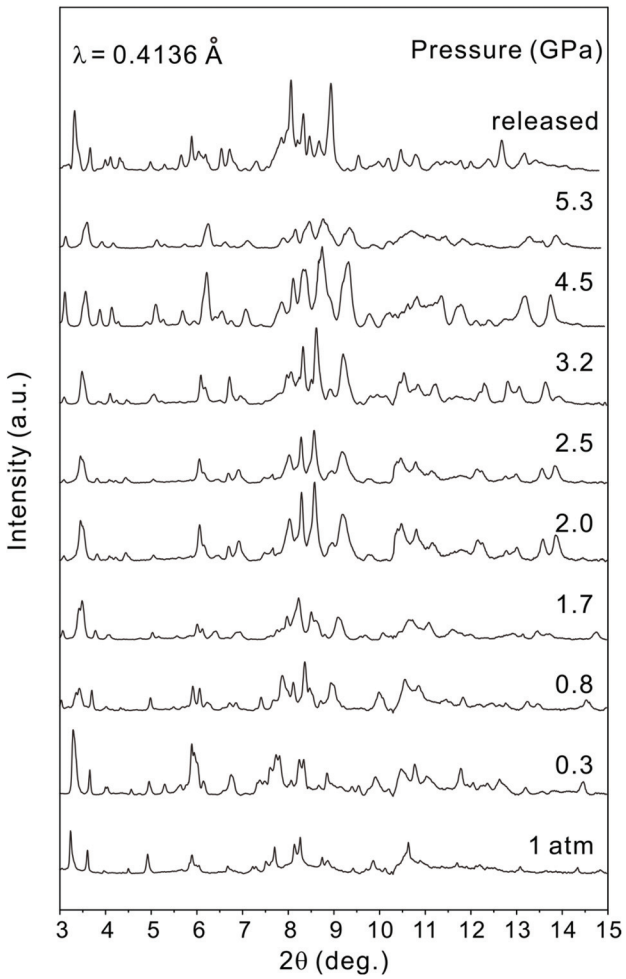


**Fig. 4** XRD patterns of the $FA_\alpha PbBr_{2+\alpha}$ composite perovskite with varying the pressure from 1 atm to 5.3 GPa.

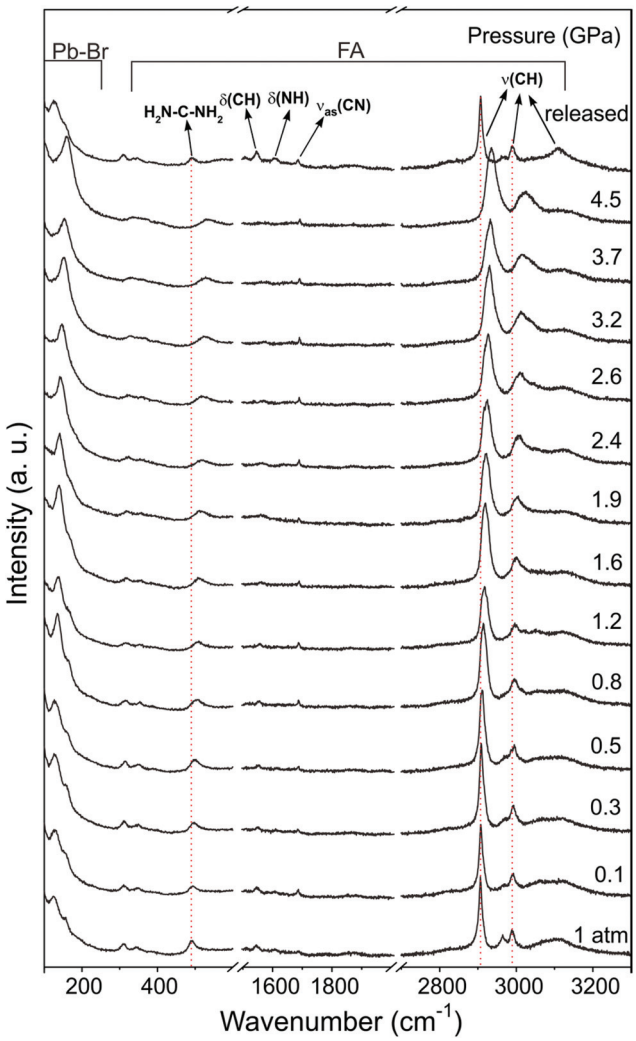


**Fig. 5** Plots of *in situ* high pressure Raman spectra of the $FA_\alpha PbBr_{2+\alpha}$ composite perovskite.

and $FA_4PbBr_6$) were conformed within a lattice mismatching of less than 1%.

The changes in Pb–Br networks had a central impact on the phase transition of the $FA_\alpha PbBr_{2+\alpha}$ composite perovskite. High-pressure *in situ* Raman experiments were performed to investigate the dynamics of the organic $FA^+$ cation and the inorganic $[PbBr_6]^{4-}$ octahedra during the compression. As shown in Fig. 5, the characteristic Raman peaks of FA and Pb–Br bonds successively shifted to the higher wavenumber, which presents the decreased bond length of Pb–Br and FA by compression. Broadening of vibrational peaks is due to an amorphorization which resulted from the large distortion of FA cations under high pressure.[33,34]

All data shown above revealed that PL enhancement of the $FA_\alpha PbBr_{2+\alpha}$ composite perovskite during the compression mainly originated from 3D $FAPbBr_3$ passivated by 0D $FA_4PbBr_6$. The original cubic structure of the $FAPbBr_3$ crystal was distorted to the orthorhombic structure with increasing pressure to 2.0 GPa, which leads to the enhancement of PL with a factor of $f$ = 21. While $FAPbBr_3$ exhibited a strong PL enhancement by phase transitions, $FA_4PbBr_6$ did not directly contribute to the PL enhancement, but was stabilized $FAPbBr_3$ by endotaxy passivation. XRD analysis showed that the lattice mismatch was kept low (<1%) during the phase transition of $FAPbBr_3$ by compression. Because of the endotaxy passivation, $FAPbBr_3$ exhibited the same pressure-induced PL changes for the subsequent multiple compression cycles (Fig. S5†).

## Conclusions

In summary, 0D–3D $FA_\alpha PbBr_{2+\alpha}$ composite perovskites have been synthesized by a solid state reaction, and their optical properties under high pressure have been investigated. The PL of $FA_\alpha PbBr_{2+\alpha}$ composite perovskites was tuned from 542 nm to 589 nm with the narrow FWHM around 20 nm by compression. Due to the endotaxy passivation of $FAPbBr_3$ by $FA_4PbBr_6$, the $FAPbBr_3$ crystal structure was reversibly

deformed by compression from an original cubic to an orthorhombic structure without agglomeration, which led to significant enhancement of PL intensity with a factor of $f = 21$. In this case, $FA_4PbBr_6$ stabilized $FAPbBr_3$ rather than directly contributing PL enhancement. Our findings provide clues for stable and optimized optoelectronic devices based on metal halide perovskites.

## Conflicts of interest

There are no conflicts to declare.

## Acknowledgements

This research was supported by Basic Science Research Program through the National Research Foundation of Korea (NRF) funded by the Ministry of Education, Science and Technology (NRF-2016K1A4A3914691, 2012R1A6A1029029 and 2017K2A9A1A06037779). High pressure experiments were performed at GeoSoilEnviroCARS (Sector 13), Partnership for Extreme Crystallography program (PX^2), Advanced Photon Source (APS), and Argonne National Laboratory. GeoSoilEnviroCARS is supported by the National Science Foundation-Earth Sciences (EAR-1634415) and Department of Energy-Geosciences (DE-FG02-94ER14466). The PX^2 program is supported by COMPRES under NSF Cooperative Agreement EAR-1661511. The use of the Advanced Photon Source was supported by the US Department of Energy, Office of Science, Office of Basic Energy Sciences, under Contract No. DE-C02-6CH11357. This work was performed at SPring-8, Japan (Proposal No. 2017B059), and partially at 4C and 9A beamlines at Pohang Accelerator Laboratory (PAL), Korea. The authors thank S. Kawaguchi for their assistance during experiments on SPring-8.



## Notes and references

1 A. Kojima, K. Teshima, Y. Shirai and T. Miyasaka, *J. Am. Chem. Soc.*, 2009, **131**, 6050–6051.
2 M. M. Lee, J. Teuscher, T. Miyasaka, T. N. Murakami and H. J. Snaith, *Science*, 2012, 1228604.
3 A. Kojima, M. Ikegami, K. Teshima and T. Miyasaka, *Chem. Lett.*, 2012, **41**, 397–399.
4 H.-S. Kim, C.-R. Lee, J.-H. Im, K.-B. Lee, T. Moehl, A. Marchioro, S.-J. Moon, R. Humphry-Baker, J.-H. Yum and J. E. Moser, *Sci. Rep.*, 2012, **2**, 591.
5 J. Burschka, N. Pellet, S.-J. Moon, R. Humphry-Baker, P. Gao, M. K. Nazeeruddin and M. Grätzel, *Nature*, 2013, **499**, 316.
6 H. J. Snaith, *J. Phys. Chem. Lett.*, 2013, **4**, 3623–3630.
7 S. Ananthakumar, J. R. Kumar and S. M. Babu, *J. Photonics Energy*, 2016, **6**, 042001.
8 B. Saparov and D. B. Mitzi, *Chem. Rev.*, 2016, **116**, 4558–4596.
9 Y. Zhang, M. I. Saidaminov, I. Dursun, H. Yang, B. Murali, E. Alarousu, E. Yengel, B. A. Alshankiti, O. M. Bakr and O. F. Mohammed, *J. Phys. Chem. Lett.*, 2017, **8**, 961–965.
10 Y. Kim, E. Yassitepe, O. Voznyy, R. Comin, G. Walters, X. Gong, P. Kanjanaboos, A. F. Nogueira and E. H. Sargent, *ACS Appl. Mater. Interfaces*, 2015, **7**, 25007–25013.
11 L. Protesescu, S. Yakunin, M. I. Bodnarchuk, F. Krieg, R. Caputo, C. H. Hendon, R. X. Yang, A. Walsh and M. V. Kovalenko, *Nano Lett.*, 2015, **15**, 3692–3696.
12 M. I. Saidaminov, J. Almutlaq, S. Sarmah, I. Dursun, A. A. Zhumekenov, R. Begum, J. Pan, N. Cho, O. F. Mohammed and O. M. Bakr, *ACS Energy Lett.*, 2016, **1**, 840–845.
13 F. Zhang, H. Zhong, C. Chen, X.-g. Wu, X. Hu, H. Huang, J. Han, B. Zou and Y. Dong, *ACS Nano*, 2015, **9**, 4533–4542.
14 J. Xu, S. Xu, Z. Qi, C. Wang, C. Lu and Y. Cui, *Nanoscale*, 2018, **10**, 10383–10388.
15 A. Jaffe, Y. Lin and H. I. Karunadasa, *ACS Energy Lett.*, 2017, **2**, 1549–1555.
16 L. Wang, K. Wang and B. Zou, *J. Phys. Chem. Lett.*, 2016, **7**, 2556–2562.
17 A. Jaffe, Y. Lin, W. L. Mao and H. I. Karunadasa, *J. Am. Chem. Soc.*, 2017, **139**, 4330–4333.
18 P. Wang, J. Guan, D. T. Galeschuk, Y. Yao, C. F. He, S. Jiang, S. Zhang, Y. Liu, M. Jin and C. Jin, *J. Phys. Chem. Lett.*, 2017, **8**, 2119–2125.
19 G. Xiao, Y. Cao, G. Qi, L. Wang, C. Liu, Z. Ma, X. Yang, Y. Sui, W. Zheng and B. Zou, *J. Am. Chem. Soc.*, 2017, **139**, 10087–10094.
20 P. Postorino and L. Malavasi, *J. Phys. Chem. Lett.*, 2017, **8**, 2613–2622.
21 E. Ryu, S. Kim, E. Jang, S. Jun, H. Jang, B. Kim and S.-W. Kim, *Chem. Mater.*, 2009, **21**, 573–575.
22 S. A. Ivanov, A. Piryatinski, J. Nanda, S. Tretiak, K. R. Zavadil, W. O. Wallace, D. Werder and V. I. Klimov, *J. Am. Chem. Soc.*, 2007, **129**, 11708–11719.
23 L.-D. Zhao, J. He, S. Hao, C.-I. Wu, T. P. Hogan, C. Wolverton, V. P. Dravid and M. G. Kanatzidis, *J. Am. Chem. Soc.*, 2012, **134**, 16327–16336.
24 Z. Ning, X. Gong, R. Comin, G. Walters, F. Fan, O. Voznyy, E. Yassitepe, A. Buin, S. Hoogland and E. H. Sargent, *Nature*, 2015, **523**, 324.
25 L. N. Quan, R. Quintero-Bermudez, O. Voznyy, G. Walters, A. Jain, J. Z. Fan, X. Zheng, Z. Yang and E. H. Sargent, *Adv. Mater.*, 2017, **29**, 1605945.
26 D. N. Minh, J. Kim, J. Hyon, J. H. Sim, H. H. Sowlih, C. Seo, J. Nam, S. Eom, S. Suk and S. Lee, *Chem. Mater.*, 2017, **29**, 5713–5719.
27 L. Protesescu, S. Yakunin, M. I. Bodnarchuk, F. Bertolotti, N. Masciocchi, A. Guagliardi and M. V. Kovalenko, *J. Am. Chem. Soc.*, 2016, **138**, 14202–14205.
28 L. Wu, H. Hu, Y. Xu, S. Jiang, M. Chen, Q. Zhong, D. Yang, Q. Liu, Y. Zhao and B. Sun, *Nano Lett.*, 2017, **17**, 5799–5804.

 

29 J. Tauc, R. Grigorovici and A. Vancu, *Phys. Status Solidi B*, 1966, **15**, 627–637.
30 A. M. Smith and S. Nie, *Acc. Chem. Res.*, 2009, **43**, 190–200.
31 D. Li, G. Wang, H.-C. Cheng, C.-Y. Chen, H. Wu, Y. Liu, Y. Huang and X. Duan, *Nat. Commun.*, 2016, **7**, 11330.
32 T. Yin, Y. Fang, W. K. Chong, K. T. Ming, S. Jiang, X. Li, J. L. Kuo, J. Fang, T. C. Sum and T. J. White, *Adv. Mater.*, 2018, **30**, 1705017.
33 L. Wang, K. Wang, G. Xiao, Q. Zeng and B. Zou, *J. Phys. Chem. Lett.*, 2016, **7**, 5273–5279.
34 R. G. Niemann, A. G. Kontos, D. Palles, E. I. Kamitsos, A. Kaltzoglou, F. Brivio, P. Falaras and P. J. Cameron, *J. Phys. Chem. C*, 2016, **120**, 2509–2519.